

Article

Assessing the Functional Redundancy between P-gp and BCRP in Controlling the Brain Distribution and Biliary Excretion of Dual Substrates with PET Imaging in Mice

Irene Hernández-Lozano ¹, Severin Mairinger ^{1,2}, Alexander Traxl ², Michael Sauberer ^{2,3}, Thomas Filip ^{2,4}, Johann Stanek ^{2,3}, Claudia Kuntner ^{2,3}, Thomas Wanek ^{2,3} and Oliver Langer ^{1,2,3,*}

¹ Department of Clinical Pharmacology, Medical University of Vienna, 1090 Vienna, Austria; irene.hernandezlozano@meduniwien.ac.at (I.H.-L.); severin.mairinger@meduniwien.ac.at (S.M.)

² Preclinical Molecular Imaging, AIT Austrian Institute of Technology GmbH, 2444 Seibersdorf, Austria; alexander.traxl@gmail.com (A.T.); michael.sauberer@meduniwien.ac.at (M.S.); thomas.filip@meduniwien.ac.at (T.F.); johann.stanek@meduniwien.ac.at (J.S.); claudia.kuntner-hannes@meduniwien.ac.at (C.K.); thomas.wanek@meduniwien.ac.at (T.W.)

³ Department of Biomedical Imaging and Image-Guided Therapy, Medical University of Vienna, 1090 Vienna, Austria

⁴ Center of Biomedical Research, Medical University of Vienna, 1090 Vienna, Austria

* Correspondence: oliver.langer@meduniwien.ac.at; Tel.: +43-(0)-40400-29810



Citation: Hernández-Lozano, I.; Mairinger, S.; Traxl, A.; Sauberer, M.; Filip, T.; Stanek, J.; Kuntner, C.; Wanek, T.; Langer, O. Assessing the Functional Redundancy between P-gp and BCRP in Controlling the Brain Distribution and Biliary Excretion of Dual Substrates with PET Imaging in Mice. *Pharmaceutics* **2021**, *13*, 1286. <https://doi.org/10.3390/pharmaceutics13081286>

Academic Editor: Stefan Oswald

Received: 16 July 2021

Accepted: 16 August 2021

Published: 18 August 2021

Publisher's Note: MDPI stays neutral with regard to jurisdictional claims in published maps and institutional affiliations.



Copyright: © 2021 by the authors. Licensee MDPI, Basel, Switzerland. This article is an open access article distributed under the terms and conditions of the Creative Commons Attribution (CC BY) license (<https://creativecommons.org/licenses/by/4.0/>).

Abstract: P-glycoprotein (P-gp) and breast cancer resistance protein (BCRP) are co-localized at the blood–brain barrier, where they display functional redundancy to restrict the brain distribution of dual P-gp/BCRP substrate drugs. We used positron emission tomography (PET) with the metabolically stable P-gp/BCRP substrates [¹¹C]tariquidar, [¹¹C]erlotinib, and [¹¹C]elacridar to assess whether a similar functional redundancy as at the BBB exists in the liver, where both transporters mediate the biliary excretion of drugs. Wild-type, *Abcb1a/b*^(-/-), *Abcg2*^(-/-), and *Abcb1a/b*^(-/-)*Abcg2*^(-/-) mice underwent dynamic whole-body PET scans after i.v. injection of either [¹¹C]tariquidar, [¹¹C]erlotinib, or [¹¹C]elacridar. Brain uptake of all three radiotracers was markedly higher in *Abcb1a/b*^(-/-)*Abcg2*^(-/-) mice than in wild-type mice, while only moderately changed in *Abcb1a/b*^(-/-) and *Abcg2*^(-/-) mice. The transfer of radioactivity from liver to excreted bile was significantly lower in *Abcb1a/b*^(-/-)*Abcg2*^(-/-) mice and almost unchanged in *Abcb1a/b*^(-/-) and *Abcg2*^(-/-) mice (with the exception of [¹¹C]erlotinib, for which biliary excretion was also significantly reduced in *Abcg2*^(-/-) mice). Our data provide evidence for redundancy between P-gp and BCRP in controlling both the brain distribution and biliary excretion of dual P-gp/BCRP substrates and highlight the utility of PET as an upcoming tool to assess the effect of transporters on drug disposition at a whole-body level.

Keywords: P-glycoprotein; breast cancer resistance protein; functional redundancy; liver; brain; PET imaging; pharmacokinetic modeling

1. Introduction

The adenosine triphosphate-binding cassette (ABC) transporters P-glycoprotein (P-gp, encoded in humans by the *ABCB1* gene and in rodents by the *Abcb1a* and *Abcb1b* genes, and breast cancer resistance protein (BCRP, encoded in humans by the *ABCG2* gene and in rodents by the *Abcg2* gene) are two important efflux transporters that are widely expressed throughout the body [1]. These two membrane transporters have a broad and largely overlapping substrate spectrum, including a variety of clinically used drugs, such as most molecularly targeted anticancer drugs [2,3]. At the luminal membrane of brain capillary endothelial cells, which form the blood–brain barrier (BBB), P-gp and BCRP play a vital defense role by limiting the distribution of their substrates into the brain by efflux transport from the endothelial cells back into the blood [4]. Several studies have provided evidence

for functional redundancy between P-gp and BCRP in limiting the brain distribution of dual P-gp/BCRP substrates [2–6]. In absence of either P-gp alone or BCRP alone, the remaining transport capacity of the other transporter usually suffices to restrict the brain access of dual substrates so that dual P-gp/BCRP substrates only gain unrestricted brain access when both transporters are absent or inhibited [4]. Using individual and combined *Abcb1a/b* and *Abcg2* knockout mice, this functional redundancy between P-gp and BCRP at the BBB has been demonstrated for several dual P-gp/BCRP substrates, such as lapatinib, erlotinib, flavopiridol, and mitoxantrone [5,6]. There is also evidence that a similar functional redundancy between P-gp and BCRP exists at the human BBB [7]. In addition, P-gp and BCRP may become overexpressed in certain tumors, in which they can contribute to multidrug resistance by limiting cellular entry of anticancer drugs [8].

Apart from the BBB, P-gp and BCRP are also expressed in excretory organs, such as the liver, the small intestine, and the kidneys [1]. At the canalicular (bile-facing) membrane of hepatocytes, P-gp and BCRP have been shown to mediate the excretion of drugs and their metabolites into bile [1]. However, it is currently incompletely understood whether the P-gp/BCRP functional redundancy observed at the BBB also extends to the biliary excretion of dual P-gp/BCRP substrates.

Positron emission tomography (PET) is a non-invasive nuclear imaging method that enables measurement of the pharmacokinetics (PK) of radiolabeled drug molecules in different tissues and organs of the body [9]. Due to the limited field of view of most currently available clinical PET scanners, dynamic PET imaging in humans has thus far been mainly limited to a short axial segment of the body (approximately 20 cm). On the other hand, small-animal PET imaging in mice offers the possibility to simultaneously and dynamically measure the whole-body disposition of radiolabeled molecules. In combination with suitable PK models, quantitative parameters can be obtained that can be related to membrane transporter activity in different organs [10]. The carbon-11 (^{11}C)-labeled third-generation P-gp inhibitors [^{11}C]tariquidar and [^{11}C]elacridar and the tyrosine kinase inhibitor [^{11}C]erlotinib are dual P-gp and BCRP substrates [6,7,11] and have been used to assess the activity of P-gp and BCRP at the human and mouse BBB [7,11–17]. All three radiotracers are predominantly excreted via the hepatobiliary route [18,19].

The aim of this study was to assess whether the functional redundancy between P-gp and BCRP observed in mice for restricting the brain distribution of [^{11}C]tariquidar, [^{11}C]erlotinib, and [^{11}C]elacridar also occurs with respect to their biliary excretion. We used previously published data sets, in which wild-type, *Abcb1a/b*^(-/-), *Abcg2*^(-/-), and *Abcb1a/b*^(-/-)*Abcg2*^(-/-) mice had been scanned with all three radiotracers [11,16]. Here, we exploited the ability of small-animal PET to perform dynamic whole-body imaging in mice, which enabled us to obtain quantitative PK parameters describing both the brain distribution and the biliary excretion of the three radiotracers in the four investigated mouse strains.

2. Materials and Methods

The data sets used for this study were previously published by Bankstahl et al. and Traxl et al. [11,16]. All animal experiments were approved by the national authorities (Amt der Niederösterreichischen Landesregierung), and all study procedures were performed in accordance with the European Communities Council Directives of 24 November 1986 (86/609/EEC) and 22 September 2010 (2010/63/EU).

2.1. Radiotracer Synthesis and Formulation

[^{11}C]Tariquidar, [^{11}C]erlotinib, and [^{11}C]elacridar were synthesized as previously reported [20–22]. For intravenous (i.v.) injection into animals, [^{11}C]tariquidar and [^{11}C]elacridar were formulated in a mixture of 0.9% aqueous saline/ethanol/polyethylene glycol 300 (50:15:35, v/v/v) [11] and [^{11}C]erlotinib was formulated in 0.1 mM hydrochloric acid in physiologic saline [16].

2.2. PET Imaging

Female wild-type, *Abcb1a/b*^(-/-), *Abcg2*^(-/-), and *Abcb1a/b*^(-/-)*Abcg2*^(-/-) mice with a FVB genetic background underwent under isoflurane/oxygen anesthesia 60 min dynamic PET scans after i.v. injection of either [¹¹C]tariquidar (32 ± 9 MBq, corresponding to 0.20 ± 0.05 µg of unlabeled tariquidar), [¹¹C]erlotinib (27 ± 8 MBq, corresponding to 0.79 ± 0.39 µg of unlabeled erlotinib), or [¹¹C]elacridar (36 ± 8 MBq, corresponding to 0.19 ± 0.05 µg of unlabeled elacridar) using a microPET Focus 220 scanner (Siemens Medical Solutions, Knoxville, TN, USA) as previously described [11,16]. At the time of the experiments, wild-type mice weighed 23.1 ± 1.6 g, *Abcb1a/b*^(-/-) mice 21.9 ± 2.1 g, *Abcg2*^(-/-) mice 21.2 ± 3.1 g, and *Abcb1a/b*^(-/-)*Abcg2*^(-/-) mice 23.5 ± 2.7 g.

2.3. Analysis of PET Data

Images were analyzed with the software AMIDE [23]. Volumes of interest for the left ventricle of the heart (image-derived arterial blood curve), brain, liver, and intestine (representing all visible intestinal radioactivity) were manually outlined on the reconstructed PET images. Time activity curves (TACs) obtained from the selected volumes of interest were expressed as percent of injected dose per milliliter (%ID/mL), except for the intestine, for which radioactivity was expressed as %ID by multiplying the image-derived radioactivity concentration by the selected volume of interest. From the TACs, the area under the curve (AUC) was calculated using Prism 8 (GraphPad Software, La Jolla, CA, USA). In order to assess the brain distribution of [¹¹C]tariquidar, [¹¹C]erlotinib, and [¹¹C]elacridar, we applied graphical non-compartmental analysis approaches. The initial uptake clearance of radioactivity from blood into brain (CL_{uptake,brain}, mL/min/g tissue) was estimated using integration plot analysis [24,25] and the following equation:

$$\frac{X_{t,\text{brain}}}{C_{t,\text{blood}}} = \text{CL}_{\text{uptake,brain}} \times \frac{\text{AUC}_{0-t,\text{blood}}}{C_{t,\text{blood}}} + V_{E,\text{brain}} \quad (1)$$

where $X_{t,\text{brain}}$ is the amount of radioactivity per gram brain tissue at time t , $C_{t,\text{blood}}$ is the radioactivity concentration in the blood at time t (image-derived from the left ventricle of the heart), $\text{AUC}_{0-t,\text{blood}}$ is the area under the blood curve from time 0 to time t , and $V_{E,\text{brain}}$ represents the capillary space as well as the rapid adsorption/binding to the vascular surface in the brain [25]. $\text{CL}_{\text{uptake,brain}}$ is the slope (from 0.5 to 4.5 min) of a plot of $X_{t,\text{brain}}/C_{t,\text{blood}}$ versus $\text{AUC}_{0-t,\text{blood}}/C_{t,\text{blood}}$ and is estimated by performing linear regression analysis. In addition, the total brain distribution volume ($V_{T,\text{brain}}$) was calculated with Logan graphical analysis [26]. $V_{T,\text{brain}}$ equals the brain-to-blood concentration ratio at steady state. While this methodology has already been used to analyze the [¹¹C]erlotinib data set [16], the brain distribution of [¹¹C]tariquidar and [¹¹C]elacridar has previously only been described in terms of brain radioactivity concentrations and brain-to-blood concentration ratios at 25 min after radiotracer injection [11].

In addition, the intestinal clearance of radioactivity with respect to the blood concentration (CL_{intestine,blood}, mL/min) was calculated by dividing the total amount of radioactivity in the intestine at the end of the PET scan by AUC_{blood}.

2.4. Pharmacokinetic Modeling

The [¹¹C]tariquidar data set has already been previously analyzed with a three-compartment model [27,28], which was slightly modified in this work (Figure 1) and applied to all three radiotracers in order to estimate the PK parameters defining the transfer of radioactivity between the compartments. CL₁ (mL/min) represents the hepatic uptake clearance, k_2 (min⁻¹) is the rate constant describing the transfer of radioactivity from liver into the sink compartment (blood), and k_3 (min⁻¹) is the rate constant describing the transfer of radioactivity from liver into excreted bile. The model assumes that all radioactivity in the intestine represents excreted bile and that direct secretion from blood into the intestine was negligible over the short duration of the PET scan. For this assumption to be confirmed, it would be necessary to examine bile duct-cannulated mice, which is technically

challenging and was not performed in the present study. The radioactivity amount in the liver was corrected for the fraction of blood in the liver (≈ 0.25). In addition, the model accounts for radiotracer delivery via the portal vein and the hepatic artery. The radiotracer concentration in the hepatic artery was assumed to correspond to the image-derived arterial blood curve (obtained from the volume of interest placed in the left ventricle of the heart), while the concentration in the portal vein was mathematically estimated from the arterial blood and the PET data during the modeling process as previously described [28]. For modeling purposes, data were expressed in megabecquerel per milliliter (MBq/mL) for blood and liver, and in MBq for the intestine.

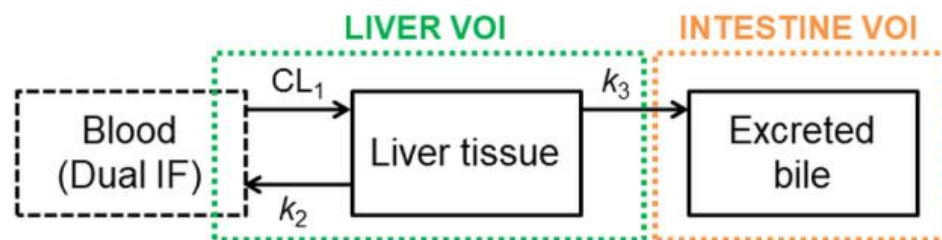


Figure 1. PK model used to assess the hepatobiliary disposition of [^{11}C]tariquidar, [^{11}C]erlotinib, and [^{11}C]elacridar. CL_1 (mL/min) represents the hepatic uptake clearance, and k_2 and k_3 (min^{-1}) are the rate constants describing the transfer of radioactivity from liver to the sink compartment (blood) and from liver to excreted bile (intestine volume of interest), respectively. The model was modified from a previously published model (Adapted from [28], AAPS, 2019). IF: input function; VOI: volume of interest.

The main difference between the already published liver model [28] and the one used in this study is related to the implementation of the input function. In the present study, the input function used was the mathematically estimated blood concentration-time curve, while the previous model used the amount of radioactivity in the hepatic sinusoids as an input function (by multiplying the mathematically estimated blood concentration curve by the volume occupied by the hepatic sinusoids—approximately 25% of the liver volume). This change leads to a different PK parameter defining the radioactivity uptake, CL_1 (mL/min) instead of k_1 (min^{-1}) [28].

2.5. Statistical Analysis

Statistical analysis was performed using Prism 8. Differences in PK parameters between mouse groups were assessed by one-way ANOVA followed by a Dunnett's multiple comparison test against the wild-type group. The level of statistical significance was set to a p -value of less than 0.05. All values are given as mean \pm standard deviation (SD).

3. Results

3.1. Functional Redundancy between P-gp and BCRP in Controlling the Brain Distribution of [^{11}C]tariquidar, [^{11}C]erlotinib, and [^{11}C]elacridar

Wild-type, $\text{Abcb1a}/b^{(-/-)}$, $\text{Abcg2}^{(-/-)}$, and $\text{Abcb1a}/b^{(-/-)}\text{Abcg2}^{(-/-)}$ mice underwent dynamic PET scans with either [^{11}C]tariquidar, [^{11}C]erlotinib, or [^{11}C]elacridar. Mean TACs in blood (image-derived blood curve), brain, liver, and intestine are shown in Supplementary Figure S1 for [^{11}C]tariquidar, in Supplementary Figure S2 for [^{11}C]erlotinib, and in Supplementary Figure S3 for [^{11}C]elacridar. In Supplementary Table S1, AUC values of the TACs in the brain and other examined tissues are given for all three radiotracers for the four mouse strains. As previously reported [11,16], brain radioactivity uptake was very low in wild-type mice for each radiotracer (Figure 2, Supplementary Table S1). Brain radioactivity uptake in $\text{Abcb1a}/b^{(-/-)}$ mice and in $\text{Abcg2}^{(-/-)}$ mice was comparably low as in wild-type mice, while a considerably higher brain uptake was observed in $\text{Abcb1a}/b^{(-/-)}\text{Abcg2}^{(-/-)}$ mice for [^{11}C]tariquidar and [^{11}C]elacridar and to a lesser extent also for [^{11}C]erlotinib.

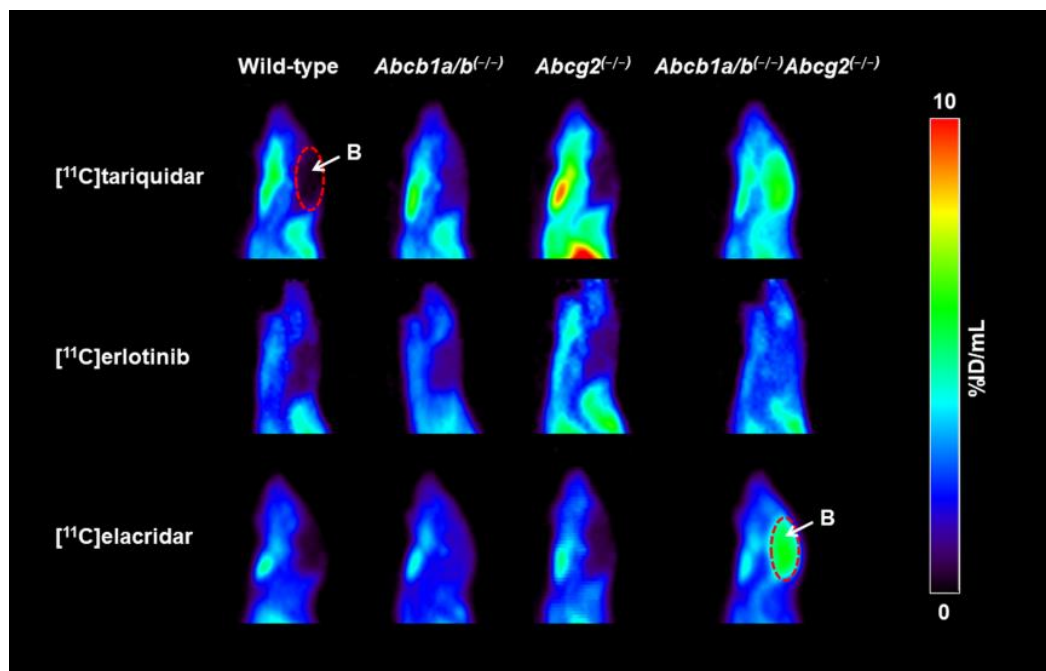


Figure 2. Sagittal PET summation images (0–60 min) of the head obtained after i.v. injection of either [^{11}C]tariquidar, [^{11}C]erlotinib, or [^{11}C]elacridar in one representative wild-type, *Abcb1a/b*^(-/-), *Abcg2*^(-/-), and *Abcb1a/b*^(-/-)*Abcg2*^(-/-) mouse. Radioactivity concentration is expressed as percent of injected dose per milliliter (%ID/mL). Brain (B) is labeled with white arrows and red dashed-line areas.

Integration plot analysis was used to estimate the initial uptake clearance of radioactivity from blood into brain ($\text{CL}_{\text{uptake,brain}}$, Figure 3, Table 1). $\text{CL}_{\text{uptake,brain}}$ was significantly increased in *Abcb1a/b*^(-/-)*Abcg2*^(-/-) mice for all three radiotracers (by 7.4-fold for [^{11}C]tariquidar, by 4.6-fold for [^{11}C]erlotinib, and by 6.2-fold for [^{11}C]elacridar), while only moderate and not significant changes were observed in *Abcb1a/b*^(-/-) mice and *Abcg2*^(-/-) mice as compared to the wild-type group. Similarly, the total brain distribution volume ($V_{\text{T,brain}}$) was significantly higher in *Abcb1a/b*^(-/-)*Abcg2*^(-/-) mice than in wild-type mice, and not significantly changed in *Abcb1a/b*^(-/-) mice and *Abcg2*^(-/-) mice for all three radiotracers (Table 1).

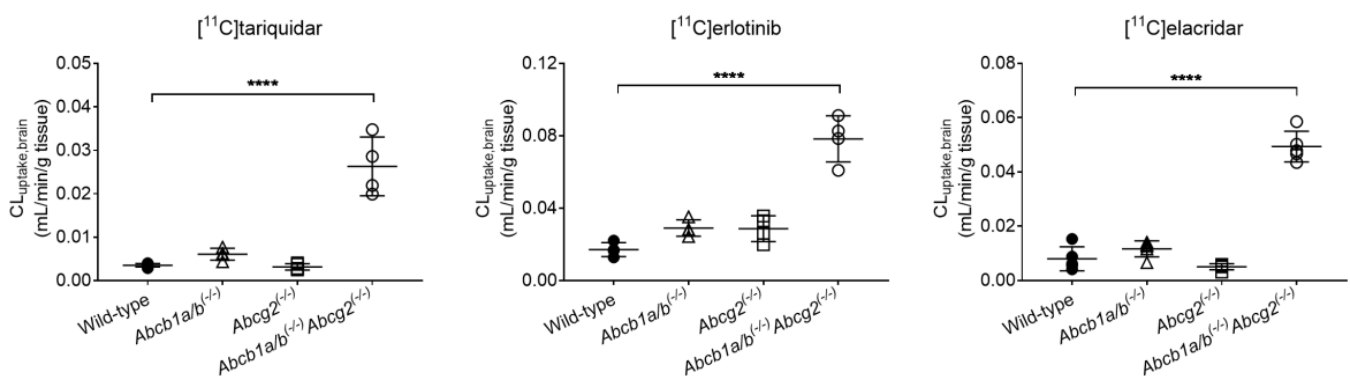


Figure 3. Initial brain uptake clearance ($\text{CL}_{\text{uptake,brain}}$) of [^{11}C]tariquidar, [^{11}C]erlotinib, and [^{11}C]elacridar determined with integration plot analysis in wild-type, *Abcb1a/b*^(-/-), *Abcg2*^(-/-), and *Abcb1a/b*^(-/-)*Abcg2*^(-/-) mice. **** $p \leq 0.0001$, one-way ANOVA followed by a Dunnett's multiple comparison test against the reference group (wild-type).

Table 1. PK parameters obtained with graphical non-compartmental analysis describing the brain distribution of [¹¹C]tariquidar, [¹¹C]erlotinib, and [¹¹C]elacridar in wild-type, *Abcb1a/b*^(-/-), *Abcg2*^(-/-), and *Abcb1a/b*^(-/-)*Abcg2*^(-/-) mice.

Radiotracer	Parameter	Wild-Type	<i>Abcb1a/b</i> ^(-/-)	<i>Abcg2</i> ^(-/-)	<i>Abcb1a/b</i> ^(-/-) <i>Abcg2</i> ^(-/-)
[¹¹ C]tariquidar	CL _{uptake,brain} (mL/min/g tissue)	0.0035 ± 0.0004	0.0061 ± 0.0014	0.0031 ± 0.0007	0.0263 ± 0.0068 *
	V _{T,brain}	0.1269 ± 0.0133	0.2169 ± 0.0227	0.1045 ± 0.0065	0.7460 ± 0.1504 *
[¹¹ C]erlotinib	CL _{uptake,brain} (mL/min/g tissue)	0.0171 ± 0.0038	0.0290 ± 0.0045	0.0287 ± 0.0071	0.0784 ± 0.0128 *
	V _{T,brain}	0.2016 ± 0.0141	0.2622 ± 0.0079	0.2335 ± 0.0174	0.5015 ± 0.0497 *
[¹¹ C]elacridar	CL _{uptake,brain} (mL/min/g tissue)	0.0080 ± 0.0044	0.0116 ± 0.0030	0.0051 ± 0.0011	0.0493 ± 0.0564 *
	V _{T,brain}	0.1547 ± 0.0489	0.2460 ± 0.0673	0.1097 ± 0.0315	0.6048 ± 0.2069 *

Data are given as mean ± SD (*n* = 4–5 per group). CL_{uptake,brain}: initial brain uptake clearance estimated with integration plot analysis; V_{T,brain}: total brain distribution volume estimated with Logan graphical analysis. * *p* ≤ 0.0001, one-way ANOVA followed by a Dunnett's multiple comparison test against the wild-type group.

3.2. Functional Redundancy between P-gp and BCRP in Mediating the Biliary Excretion of [¹¹C]tariquidar, [¹¹C]erlotinib, and [¹¹C]elacridar

Representative PET summation images of the abdominal region obtained after i.v. injection of either [¹¹C]tariquidar, [¹¹C]erlotinib, or [¹¹C]elacridar in the different mouse strains are shown in Figure 4. For each radiotracer, appreciable excretion of radioactivity into the intestine occurred in wild-type mice over the duration of the PET scan (Figure 4, Supplementary Table S1). At the end of the PET scan, the total amount of radioactivity in the intestine of wild-type mice was 17.2 ± 3.1 %ID for [¹¹C]tariquidar (Supplementary Figure S1), 60.8 ± 6.6 %ID for [¹¹C]erlotinib (Supplementary Figure S2), and 18.9 ± 0.8 %ID for [¹¹C]elacridar (Supplementary Figure S3). A decrease in the intestinal radioactivity was observed in *Abcb1a/b*^(-/-)*Abcg2*^(-/-) mice, while intestinal radioactivity in *Abcb1a/b*^(-/-) mice and *Abcg2*^(-/-) mice appeared to be similar to wild-type mice for all three radiotracers (Figure 4).

The PK model (Figure 1) was used to estimate the hepatic uptake clearance (CL₁) and the rate constants defining the transfer of radioactivity from liver into the sink compartment (blood, *k*₂) and from liver into excreted bile (*k*₃). Visually, the model provided good fits of the observed liver and intestinal TACs (Supplementary Figure S4) and parameter precision (determined as percent coefficient of variation, %CV) was acceptable (Table 2). CL₁, *k*₂, and *k*₃ values were considerably lower for [¹¹C]tariquidar and [¹¹C]elacridar than for [¹¹C]erlotinib (Table 2). No significant differences were observed for CL₁ and *k*₂ between wild-type and knockout mice for any of the studied radiotracers (Table 2). *k*₃ was significantly decreased in *Abcb1a/b*^(-/-)*Abcg2*^(-/-) mice as compared to the wild-type group, by 1.96-fold for [¹¹C]tariquidar, by 2.79-fold for [¹¹C]erlotinib, and by 2.75-fold for [¹¹C]elacridar (Figure 5). In addition, for [¹¹C]erlotinib, *k*₃ was significantly (2.11-fold) reduced in *Abcg2*^(-/-) mice relative to wild-type mice. No significant differences were observed in *k*₃ for [¹¹C]tariquidar and [¹¹C]elacridar between wild-type and single transporter knockout mice (Table 2, Figure 5).

The intestinal clearance (CL_{intestine,blood}) was significantly decreased in *Abcg2*^(-/-) and *Abcb1a/b*^(-/-)*Abcg2*^(-/-) mice as compared to the wild-type group, while it was unchanged in *Abcb1a/b*^(-/-) mice for both [¹¹C]tariquidar and [¹¹C]erlotinib (Supplementary Figure S5). No significant differences were observed in CL_{intestine,blood} for [¹¹C]elacridar between wild-type and knockout animals (Supplementary Figure S5).

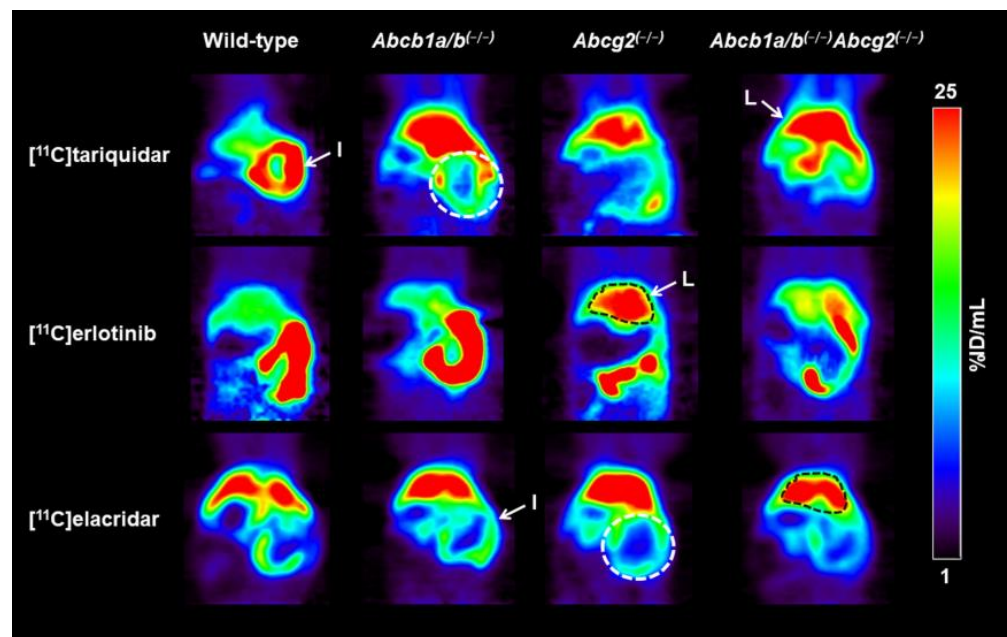


Figure 4. Coronal PET summation images (0–60 min) of the abdominal region obtained after i.v. injection of either [^{11}C]tariquidar, [^{11}C]erlotinib, or [^{11}C]elacridar in one representative wild-type, *Abcb1a/b*^(-/-), *Abcg2*^(-/-), and *Abcb1a/b*^(-/-)*Abcg2*^(-/-) mouse. Radioactivity concentration is expressed as percent of injected dose per milliliter (%ID/mL). Anatomical structures are labeled with white arrows and colored dashed-line areas (I: intestine, white; L: liver, black).

Table 2. PK parameters obtained with the compartmental model describing the hepatobiliary disposition of [^{11}C]tariquidar, [^{11}C]erlotinib, and [^{11}C]elacridar in wild-type, *Abcb1a/b*^(-/-), *Abcg2*^(-/-), and *Abcb1a/b*^(-/-)*Abcg2*^(-/-) mice.

Radiotracer	Parameter	Wild-Type	<i>Abcb1a/b</i> ^(-/-)	<i>Abcg2</i> ^(-/-)	<i>Abcb1a/b</i> ^(-/-) <i>Abcg2</i> ^(-/-)
[^{11}C]tariquidar	CL ₁ (mL/min)	2.2798 ± 0.5058 (12.9–32.3)	1.7207 ± 0.1377 (10.7–23.1)	1.5836 ± 0.1993 (9.6–22.1)	1.9316 ± 0.6933 (9.6–34.2)
	k ₂ (min ⁻¹)	0.2600 ± 0.0475 (11.0–26.4)	0.2421 ± 0.0227 (10.5–19.0)	0.3244 ± 0.0204 (9.0–20.5)	0.3441 ± 0.1549 (9.0–29.7)
	k ₃ (min ⁻¹)	0.0036 ± 0.0004 (4.1–7.6)	0.0039 ± 0.0002 (4.2–7.6)	0.0037 ± 0.0007 (2.8–9.1)	0.0019 ± 0.0004 * (5.3–8.4)
[^{11}C]erlotinib	CL ₁ (mL/min)	5.9437 ± 2.4249 (5.3–51.5)	5.2978 ± 1.8375 (12.1–45.4)	6.3856 ± 1.7690 (10.6–33.4)	7.3708 ± 0.2309 (20.7–36.7)
	k ₂ (min ⁻¹)	0.6431 ± 0.2567 (5.1–47.3)	0.5815 ± 0.1818 (10.8–41.4)	0.6051 ± 0.0664 (10.7–30.8)	0.5484 ± 0.1021 (17.6–32.2)
	k ₃ (min ⁻¹)	0.0193 ± 0.0025 (1.2–4.2)	0.0191 ± 0.0067 (1.7–4.7)	0.0091 ± 0.0011 * (1.9–3.3)	0.0069 ± 0.0018 * (2.4–4.1)
[^{11}C]elacridar	CL ₁ (mL/min)	0.5338 ± 0.1759 (6.0–14.3)	0.6887 ± 0.1939 (11.3–22.4)	0.4304 ± 0.1392 (4.0–21.0)	0.5777 ± 0.2241 (4.9–24.6)
	k ₂ (min ⁻¹)	0.1121 ± 0.0641 (7.7–13.5)	0.1872 ± 0.1165 (10.5–17.5)	0.1674 ± 0.1366 (4.8–20.6)	0.1426 ± 0.0728 (7.1–18.8)
	k ₃ (min ⁻¹)	0.0040 ± 0.0008 (4.0–6.8)	0.0042 ± 0.0008 (5.2–8.9)	0.0043 ± 0.0010 (3.2–18.6)	0.0015 ± 0.0006 * (7.0–23.3)

Data are given as mean ± SD ($n = 4\text{--}5$ per group). Values in parentheses represent the range in percent coefficient of variation (%CV), which determines the parameter precision. PK parameters were obtained with the liver PK model. CL₁ defines the hepatic uptake clearance, and k_2 and k_3 are the rate constants defining the transfer of radioactivity from liver to the sink compartment (blood) and from liver to excreted bile, respectively. * $p \leq 0.01$, one-way ANOVA followed by a Dunnett's multiple comparison test against the wild-type group.

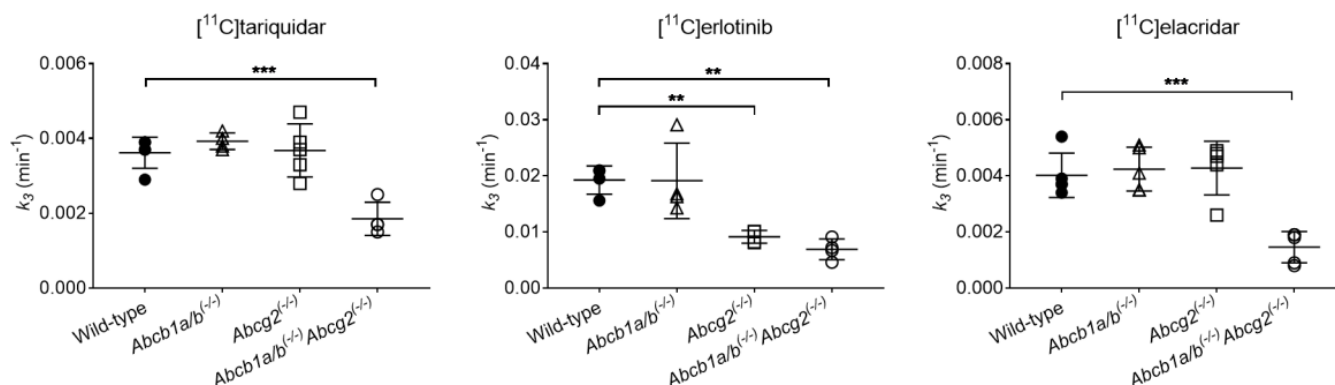


Figure 5. Rate constant (k_3) representing the transfer of radioactivity from liver to excreted bile (intestinal region of interest) obtained with the compartmental model for [¹¹C]tariquidar, [¹¹C]erlotinib, and [¹¹C]jelacridar in wild-type, *Abcb1a/b*^(-/-), *Abcg2*^(-/-), and *Abcb1a/b*^(-/-)*Abcg2*^(-/-) mice. ** $p \leq 0.01$, *** $p \leq 0.001$, one-way ANOVA followed by a Dunnett's multiple comparison test against the reference group (wild-type).

4. Discussion

P-gp and BCRP play a protective role at the BBB by limiting the entry of xenobiotics, such as drugs, from blood into the brain. Due to their co-localization and considerable overlap in substrate specificity, P-gp and BCRP display functional redundancy in the active efflux of their common substrates across the BBB [4,6]. This was shown to lead to substantial increases in the brain distribution of dual P-gp/BCRP substrates in *Abcb1a/b*^(-/-)*Abcg2*^(-/-) mice, while only small changes were observed when only one transporter is absent (*Abcb1a/b*^(-/-) mice and *Abcg2*^(-/-) mice) [2–6]. In the present study, we used whole-body PET imaging with the i.v. administered dual P-gp/BCRP substrates [¹¹C]tariquidar, [¹¹C]erlotinib, and [¹¹C]jelacridar [11,16] in wild-type, *Abcb1a/b*^(-/-), *Abcg2*^(-/-), and *Abcb1a/b*^(-/-)*Abcg2*^(-/-) mice to assess in vivo whether a similar P-gp/BCRP functional redundancy as described for the BBB also occurs at the level of the canalicular membrane of hepatocytes.

The [¹¹C]tariquidar and [¹¹C]jelacridar data used for this study have been previously analyzed to investigate the transport of both radiotracers by P-gp and BCRP at the mouse BBB [11]. In the previous study, the brain distribution of [¹¹C]tariquidar and [¹¹C]jelacridar was only assessed in terms of the PET-measured brain TACs and brain-to-blood radioactivity concentration ratios at 25 min after radiotracer injection, using blood samples taken from separate groups of animals [11]. No kinetic analysis was performed to assess the brain uptake of [¹¹C]tariquidar and [¹¹C]jelacridar. The [¹¹C]erlotinib data were previously analyzed using integration plot analysis to obtain $CL_{\text{uptake,brain}}$ as a parameter describing brain distribution of [¹¹C]erlotinib in mice [16]. In order to use the same methodology, we re-analyzed the [¹¹C]tariquidar and [¹¹C]jelacridar data using integration plot and Logan analysis to estimate $CL_{\text{uptake,brain}}$ and $V_{T,\text{brain}}$ values. To this end, an image-derived blood curve was obtained from the volume of interest placed in the left ventricle of the heart, as was previously done for [¹¹C]erlotinib [16].

In agreement with the published data [11,16], only small or no increases were observed in the brain distribution ($CL_{\text{uptake,brain}}$, $V_{T,\text{brain}}$) of the three radiotracers in the single transporter knockout animals (*Abcb1a/b*^(-/-) and *Abcg2*^(-/-)) (Table 1, Figure 3). For both [¹¹C]tariquidar and [¹¹C]jelacridar, brain distribution was moderately increased in *Abcb1a/b*^(-/-) mice but not increased in *Abcg2*^(-/-) mice, relative to wild-type mice. In contrast, for [¹¹C]erlotinib, the brain distribution was to a similar extent increased in both *Abcb1a/b*^(-/-) mice and *Abcg2*^(-/-) mice. This suggests that P-gp plays a greater role in limiting the brain distribution of [¹¹C]tariquidar and [¹¹C]jelacridar than that of [¹¹C]erlotinib. Moreover, a greater effect of *Abcb1a/b* knockout than of *Abcg2* knockout on the brain uptake of dual P-gp/BCRP substrates in mice may be attributed to P-gp being the quantitatively more important transporter at the mouse BBB (abundance ratio of P-gp to BCRP in brain

capillaries of wild-type mice: 3.9) [29]. In agreement with the expected behavior of dual P-gp/BCRP substrates [6], there was a substantial increase in $CL_{\text{uptake,brain}}$ and $V_{T,\text{brain}}$ in combination knockout mice ($Abcb1a/b^{(-/-)}Abcg2^{(-/-)}$) for all three radiotracers (Table 1, Figure 3). It should be noted that it cannot be excluded that apart from P-gp and BCRP additional uptake and efflux transporters influenced the brain distribution of the investigated radiotracers.

This large increase in the brain distribution of dual P-gp/BCRP substrates in $Abcb1a/b^{(-/-)}Abcg2^{(-/-)}$ mice relative to the small changes observed in the individual transporter knockout mice is in agreement with kinetic theory [30], implying that the brain distribution of dual substrates increases as an asymptotic function of the fraction excreted (f_e) by the transporter [4]. Thus, the sum of the increases in the brain distribution in the individual transporter knockouts will underpredict the increase observed in $Abcb1a/b^{(-/-)}Abcg2^{(-/-)}$ mice because the total increase in brain distribution is a nonlinear function of f_e and not an additive parameter. The mathematical relationship describing the fold change in brain distribution ($1/(1 - f_e)$) has been shown to predict the large changes in brain distribution of dual P-gp/BCRP substrates such as lapatinib in mice when both transporters were absent [4].

In order to study hepatobiliary excretion of the three radiolabeled P-gp/BCRP substrates, we analyzed the PET data with a liver PK model that was slightly modified from a previously developed model [28]. Although the [^{11}C]tariquidar PET data have already been analyzed with another liver PK model [27], a re-analysis of the data was done with the modified PK model to enable a direct comparison with the other two radiotracers. In addition, integration plot analysis has previously been applied to assess the influence of P-gp and BCRP on the biliary excretion of [^{11}C]erlotinib in mice [16]. Although integration plot analysis provided similar results for [^{11}C]erlotinib as in this study, it does not provide a complete picture of the hepatobiliary disposition of a radiotracer [10]. Moreover, the liver PK model used in this study considers the dual blood input to the liver via the portal vein and the hepatic artery. The radiotracer concentration in the hepatic artery was assumed to be the same as the radiotracer concentration derived from the volume of interest placed in the left ventricle of the heart, while the concentration in the portal vein, which is expected to be different from the arterial concentration, was mathematically estimated as previously described [31]. In addition, the PK model assumes that radiotracer is not metabolized during the PET scan. This is supported by previous studies in wild-type mice, in which the majority of radioactivity in plasma, brain, and liver after i.v. injection of [^{11}C]tariquidar, [^{11}C]erlotinib, or [^{11}C]elacridar was found to be in the form of unmetabolized radiotracer (percentage of unchanged radiotracer at 25–30 min after radiotracer injection, plasma: 78.3% ([^{11}C]tariquidar), 90.3% ([^{11}C]erlotinib), 95.8% ([^{11}C]elacridar); brain: 88.8% ([^{11}C]erlotinib), 95.4% ([^{11}C]elacridar); liver: 92.8% ([^{11}C]tariquidar), 74.8% ([^{11}C]erlotinib)) [14,27,32].

In agreement with previous kinetic analysis [27], the value of k_3 (representing biliary excretion) was significantly decreased for [^{11}C]tariquidar in $Abcb1a/b^{(-/-)}Abcg2^{(-/-)}$ mice, while it remained unchanged in both $Abcb1a/b^{(-/-)}$ mice and $Abcg2^{(-/-)}$ mice (Figure 5, Table 2). Similarly, [^{11}C]elacridar showed minimal changes in k_3 in both individual transporter knockout mouse groups as compared to wild-type mice, while k_3 was significantly decreased in $Abcb1a/b^{(-/-)}Abcg2^{(-/-)}$ mice. This suggests that, similar to [^{11}C]tariquidar, the biliary excretion of [^{11}C]elacridar is mediated by both P-gp and BCRP. Accordingly, k_3 for [^{11}C]erlotinib was also significantly decreased in $Abcb1a/b^{(-/-)}Abcg2^{(-/-)}$ mice, similar to the previously reported reduction in k_{bile} estimated with integration plot analysis [16]. However, k_3 was also significantly and to a similar extent reduced in $Abcg2^{(-/-)}$ mice as compared to wild-type mice, while no significant changes were observed for k_3 in $Abcb1a/b^{(-/-)}$ mice (Figure 5, Table 2). This suggests that although both P-gp and BCRP contribute to the efflux of [^{11}C]erlotinib at the mouse BBB, BCRP mainly mediates the biliary excretion of [^{11}C]erlotinib in the mouse liver, with only a minor contribution of P-gp. These differences among the radiotracers may be ascribed to different affinities (K_m) and transport capacities (V_{max}) by P-gp and BCRP. A detailed assessment would require the

performance of comparative in vitro saturation experiments in transporter-overexpressing cell lines.

The same kinetic theory used for the brain distribution of dual P-gp/BCRP substrates can be applied to predict the fold change in biliary excretion of dual substrates [30]. Thus, the loss of function of only one transporter will have minor consequences, while the loss of function of both transporters will lead to an exponential decrease in biliary excretion. This may have direct consequences for the risk of occurrence of transporter-mediated drug–drug interactions (DDIs) for dual P-gp/BCRP substrate drugs at the level of the canalicular hepatocyte membrane [1]. Similar to the brain [4], significant changes in hepatic drug disposition are only expected to occur when both transporters are simultaneously inhibited. As few clinically used drugs are likely to inhibit both P-gp and BCRP simultaneously, it appears rather unlikely that dual P-gp/BCRP substrate drugs become victims of P-gp- and BCRP-mediated DDIs in the liver, due to the functional redundancy between these two transporters. For all three investigated radiotracers, the fold decrease in biliary excretion was not as great as the fold increase in their brain uptake in *Abcb1a/b*^(-/-)*Abcg2*^(-/-) mice, indicating that the combined fractions of radiotracer excreted by P-gp and BCRP at the canalicular membrane of hepatocytes are not much greater than 0.5 [30]. This may be potentially related to an additional involvement of other transporters in the biliary excretion of the investigated radiotracers.

An alternative explanation for the only moderate changes in brain uptake or biliary excretion of the dual P-gp/BCRP substrates in single transporter knockout mice could be a compensatory upregulation of P-gp in *Abcg2*^(-/-) mice or an upregulation of BCRP in *Abcb1a/b*^(-/-) mice. However, it has been shown before by means of quantitative proteomics that there are no changes in the abundance of P-gp, BCRP, and other ABC and solute carrier (SLC) transporters in brain capillary endothelial cells of the same knockout mouse models as used in this study [33]. This supports that the functional redundancy between P-gp and BCRP observed at the mouse BBB is not related to compensatory changes in transporter expression. On the other hand, quantitative proteomics data for transporter expression in the liver of the investigated transporter knockout mouse models are currently not available. One study showed that no overexpression of *Abcg2* mRNA occurs in the liver of the same *Abcb1a/b*^(-/-) mouse model as used in this study [34]. However, mRNA levels do not always correlate with protein abundance, and highly expressed proteins may not require high expression levels of mRNA. In addition, mRNA expression of *Abcb1a* and protein expression of P-gp (ABCB1A) in the liver of the *Abcg2*^(-/-) mouse model have been investigated [35]. While *Abcb1a* mRNA expression was unchanged in *Abcg2*^(-/-) mice, there was a significant, approximately twofold increase in the hepatic abundance of ABCB1A protein in *Abcg2*^(-/-) mice. This could imply that compensatory P-gp upregulation may have at least partly contributed to the lack of changes in *k*₃ of [¹¹C]tariquidar and [¹¹C]elacridar in *Abcg2*^(-/-) mice. Thus, although similar effects as observed at the BBB were observed in the biliary excretion of dual P-gp/BCRP substrates, suggesting functional redundancy between these two transporters at the canalicular membrane of hepatocytes, a contribution of compensatory transporter upregulation cannot be entirely discarded.

It further remains to be determined whether similar effects as in mice occur in human hepatocytes, which differ from rodents in terms of the relative abundances of different membrane transporters [36]. PET studies with radiolabeled P-gp/BCRP substrates may be helpful to answer these questions in humans [27]. The upcoming availability of total-body PET scanners with large axial fields of view of up to 200 cm [37] will provide the unprecedented possibility to simultaneously assess the effects of transporters on drug disposition in humans in several different organs, such as the brain and the liver, or in primary tumors and metastases.

5. Conclusions

In this study, we evaluated whether the known functional redundancy between P-gp and BCRP at the BBB also extends to the canalicular membrane of hepatocytes,

where both transporters mediate the biliary excretion of drugs and their metabolites. To this end, we performed PET scans with the three metabolically stable dual P-gp/BCRP substrates [^{11}C]tariquidar, [^{11}C]erlotinib, and [^{11}C]elacridar in wild-type, *Abcb1a/b*^(-/-), *Abcg2*^(-/-), and *Abcb1a/b*^(-/-)*Abcg2*^(-/-) mice. Using different PK analysis approaches, we observed that brain distribution and biliary excretion of the three studied radiotracers was markedly changed in *Abcb1a/b*^(-/-)*Abcg2*^(-/-) mice as compared to wild-type mice, while only moderate changes were observed when only one of the two transporters was absent. Altogether, our data suggest functional redundancy between P-gp and BCRP both in controlling the brain distribution and the biliary excretion of dual P-gp/BCRP substrates, which may point to a low risk for the occurrence of transporter-mediated DDIs. Our study highlights the potential of PET imaging for assessing the effects of transporters on drug disposition on a whole-body level.

Supplementary Materials: The following are available online at <https://www.mdpi.com/article/10.3390/pharmaceutics13081286/s1>, Table S1: Area under the curve (AUC) values. Figure S1: Mean time-activity curves of [^{11}C]tariquidar. Figure S2: Mean time-activity curves of [^{11}C]erlotinib. Figure S3: Mean time-activity curves of [^{11}C]elacridar. Figure S4: Observed and fitted time-activity curves of [^{11}C]tariquidar, [^{11}C]erlotinib, and [^{11}C]elacridar in representative subjects. Figure S5: Intestinal clearance ($\text{CL}_{\text{intestine,blood}}$).

Author Contributions: Conceptualization, O.L.; methodology, I.H.-L., A.T., C.K. and T.W.; software, I.H.-L.; formal analysis, I.H.-L., A.T. and T.W.; investigation, I.H.-L., A.T., S.M., M.S., T.F., J.S. and C.K.; resources, T.W. and C.K.; writing—original draft preparation, I.H.-L. and O.L.; writing—review and editing, all authors; visualization, I.H.-L. and O.L.; supervision, O.L. and T.W.; project administration, O.L. and T.W.; funding acquisition, O.L. All authors have read and agreed to the published version of the manuscript.

Funding: Open Access Funding by the Austrian Science Fund (FWF), grant numbers KLI 694-B30 and F 3513-B20; the Gesellschaft für Forschungsförderung Niederösterreich, grant number LSC15-003; and the European Community's Seventh Framework Programme (FP7/2007-2013), grant number 201380.

Institutional Review Board Statement: All animal experiments were approved by the national authorities (Amt der Niederösterreichischen Landesregierung), and all study procedures were performed in accordance with the European Communities Council Directives of 24 November 1986 (86/609/EEC) and 22 September 2010 (2010/63/EU).

Informed Consent Statement: Not applicable.

Data Availability Statement: The data presented in this study are available on request from the corresponding author.

Acknowledgments: The authors would like to thank Mathilde Löbsch for technical assistance.

Conflicts of Interest: The authors declare no conflict of interest. The funders had no role in the design of the study; in the collection, analyses, or interpretation of data; in the writing of the manuscript, or in the decision to publish the results.

Abbreviations

ABC (ATP-binding cassette), BBB (blood–brain barrier), BCRP (breast cancer resistance protein), DDI (drug–drug interaction), f_e (fraction excreted), i.v. (intravenous), PET (positron emission tomography), P-gp (P-glycoprotein), PK (pharmacokinetic(s)), TAC (time-activity curve).

References

1. Giacomini, K.; Huang, S.; Tweedie, D. Membrane transporters in drug development. *Nat. Rev. Drug Discov.* **2010**, *9*, 215–236.
2. Agarwal, S.; Hartz, A.M.S.; Elmquist, E.F.; Bauer, B. Breast cancer resistance protein and p-glycoprotein in brain cancer: Two gatekeepers team up. *Curr. Pharm. Des.* **2011**, *17*, 2793–2802. [[CrossRef](#)] [[PubMed](#)]
3. Durmus, S.; Hendrikx, J.J.; Schinkel, A.H. Apical ABC transporters and cancer chemotherapeutic drug disposition. *Adv. Cancer Res.* **2015**, *125*, 1–41. [[PubMed](#)]

4. Kalvass, J.C.; Polli, J.W.; Bourdet, D.L.; Feng, B.; Huang, S.M.; Liu, X.; Smith, Q.R.; Zhang, L.K.; Zamek-Gliszczynski, M.J.; International Transporter, C. Why clinical modulation of efflux transport at the human blood-brain barrier is unlikely: The ITC evidence-based position. *Clin. Pharmacol. Ther.* **2013**, *94*, 80–94. [[CrossRef](#)] [[PubMed](#)]
5. Polli, J.W.; Olson, K.L.; Chism, J.P.; John-Williams, L.S.; Yeager, R.L.; Woodard, S.M.; Otto, V.; Castellino, S.; Demby, V.E. An unexpected synergist role of P-glycoprotein and breast cancer resistance protein on the central nervous system penetration of the tyrosine kinase inhibitor lapatinib (N-(3-chloro-4-((3-fluorobenzyl)oxy)phenyl)-6-[5-((2-(methylsulfonyl)ethyl)amino)methyl]-2-furyl]-4-quinazolinamine; GW572016). *Drug Metab. Dispos.* **2009**, *37*, 439–442. [[PubMed](#)]
6. Kodaira, H.; Kusuhara, H.; Ushiki, J.; Fuse, E.; Sugiyama, Y. Kinetic analysis of the cooperation of P-glycoprotein (P-gp/Abcb1) and breast cancer resistance protein (Bcrp/Abcg2) in limiting the brain and testis penetration of erlotinib, flavopiridol, and mitoxantrone. *J. Pharmacol. Exp. Ther.* **2010**, *333*, 788–796. [[CrossRef](#)]
7. Bauer, M.; Romermann, K.; Karch, R.; Wulkersdorfer, B.; Stanek, J.; Philippe, C.; Maier-Salamon, A.; Haslacher, H.; Jungbauer, C.; Wadsak, W.; et al. Pilot PET study to assess the functional interplay between ABCB1 and ABCG2 at the human blood-brain barrier. *Clin. Pharmacol. Ther.* **2016**, *100*, 131–141. [[CrossRef](#)]
8. Robey, R.W.; Pluchino, K.M.; Hall, M.D.; Fojo, A.T.; Bates, S.E.; Gottesman, M.M. Revisiting the role of ABC transporters in multidrug-resistant cancer. *Nat. Rev. Cancer* **2018**, *18*, 452–464. [[CrossRef](#)]
9. Tournier, N.; Stieger, B.; Langer, O. Imaging techniques to study drug transporter function in vivo. *Pharmacol. Ther.* **2018**, *189*, 104–122. [[CrossRef](#)]
10. Hernández Lozano, I.; Langer, O. Use of imaging to assess the activity of hepatic transporters. *Expert Opin. Drug Metab. Toxicol.* **2020**, *16*, 149–164. [[CrossRef](#)]
11. Bankstahl, J.P.; Bankstahl, M.; Römermann, K.; Wanek, T.; Stanek, J.; Windhorst, A.D.; Fedrowitz, M.; Erker, T.; Müller, M.; Löscher, W.; et al. Tariquidar and elacridar are dose-dependently transported by P-glycoprotein and Bcrp at the blood-brain barrier: A small-animal positron emission tomography and in vitro study. *Drug Metab. Dispos.* **2013**, *41*, 754–762. [[CrossRef](#)]
12. Wanek, T.; Kuntner, C.; Bankstahl, J.P.; Mairinger, S.; Bankstahl, M.; Stanek, J.; Sauberer, M.; Filip, T.; Erker, T.; Müller, M.; et al. A novel PET protocol for visualization of breast cancer resistance protein function at the blood-brain barrier. *J. Cereb. Blood Flow Metab.* **2012**, *32*, 2002–2011. [[CrossRef](#)]
13. Bauer, M.; Karch, R.; Zeitlinger, M.; Stanek, J.; Philippe, C.; Wadsak, W.; Mitterhauser, M.; Jäger, W.; Haslacher, H.; Müller, M.; et al. Interaction of [¹¹C]tariquidar and [¹¹C]elacridar with P-glycoprotein and breast cancer resistance protein at the human blood-brain barrier. *J. Nucl. Med.* **2013**, *54*, 1181–1187. [[CrossRef](#)] [[PubMed](#)]
14. Traxl, A.; Mairinger, S.; Filip, T.; Sauberer, M.; Stanek, J.; Poschner, S.; Jäger, W.; Zoufal, V.; Novarino, G.; Tournier, N.; et al. Inhibition of ABCB1 and ABCG2 at the mouse blood-brain barrier with marketed drugs to improve brain delivery of the model ABCB1/ABCG2 substrate [¹¹C]erlotinib. *Mol. Pharm.* **2019**, *16*, 1282–1293. [[CrossRef](#)] [[PubMed](#)]
15. Bauer, M.; Karch, R.; Wulkersdorfer, B.; Philippe, C.; Nics, L.; Klebermass, E.M.; Weber, M.; Poschner, S.; Haslacher, H.; Jäger, W.; et al. A proof-of-concept study to inhibit ABCG2- and ABCB1-mediated efflux transport at the human blood-brain barrier. *J. Nucl. Med.* **2019**, *60*, 486–491. [[CrossRef](#)] [[PubMed](#)]
16. Traxl, A.; Wanek, T.; Mairinger, S.; Stanek, J.; Filip, T.; Sauberer, M.; Müller, M.; Kuntner, C.; Langer, O. Breast cancer resistance protein and P-Glycoprotein influence in vivo disposition of [¹¹C]erlotinib. *J. Nucl. Med.* **2015**, *56*, 1930–1936. [[CrossRef](#)] [[PubMed](#)]
17. Tournier, N.; Goutal, S.; Mairinger, S.; Hernandez-Lozano, I.; Filip, T.; Sauberer, M.; Caille, F.; Breuil, L.; Stanek, J.; Freeman, A.F.; et al. Complete inhibition of ABCB1 and ABCG2 at the blood-brain barrier by co-infusion of erlotinib and tariquidar to improve brain delivery of the model ABCB1/ABCG2 substrate [¹¹C]erlotinib. *J. Cereb. Blood Flow Metab.* **2021**, *41*, 1634–1646. [[CrossRef](#)]
18. Ling, J.; Johnson, K.A.; Miao, Z.; Rakhit, A.; Pantze, M.P.; Hamilton, M.; Lum, B.L.; Prakash, C. Metabolism and excretion of erlotinib, a small molecule inhibitor of epidermal growth factor receptor tyrosine kinase, in healthy male volunteers. *Drug Metab. Dispos.* **2006**, *34*, 420–426. [[CrossRef](#)]
19. Bauer, M.; Blaickner, M.; Philippe, C.; Wadsak, W.; Hacker, M.; Zeitlinger, M.; Langer, O. Whole-body distribution and radiation dosimetry of [¹¹C]elacridar and [¹¹C]tariquidar in humans. *J. Nucl. Med.* **2016**, *57*, 1265–1268. [[CrossRef](#)]
20. Bauer, F.; Kuntner, C.; Bankstahl, J.P.; Wanek, T.; Bankstahl, M.; Stanek, J.; Mairinger, S.; Dörner, B.; Löscher, W.; Müller, M.; et al. Synthesis and in vivo evaluation of [¹¹C]tariquidar, a positron emission tomography radiotracer based on a third-generation P-glycoprotein inhibitor. *Bioorg. Med. Chem.* **2010**, *18*, 5489–5497. [[CrossRef](#)]
21. Philippe, C.; Mairinger, S.; Pichler, V.; Stanek, J.; Nics, L.; Mitterhauser, M.; Hacker, M.; Wanek, T.; Langer, O.; Wadsak, W. Comparison of fully-automated radiosyntheses of [¹¹C]erlotinib for preclinical and clinical use starting from in target produced [¹¹C]CO₂ or [¹¹C]CH₄. *EJNMMI Radiopharm. Chem.* **2018**, *3*, 8. [[CrossRef](#)]
22. Dörner, B.; Kuntner, C.; Bankstahl, J.P.; Bankstahl, M.; Stanek, J.; Wanek, T.; Stundner, G.; Mairinger, S.; Löscher, W.; Müller, M.; et al. Synthesis and small-animal positron emission tomography evaluation of [¹¹C]-elacridar as a radiotracer to assess the distribution of P-glycoprotein at the blood-brain barrier. *J. Med. Chem.* **2009**, *52*, 6073–6082. [[CrossRef](#)]
23. Loening, A.M.; Gambhir, S.S. AMIDE: A free software tool for multimodality medical image analysis. *Mol. Imaging* **2003**, *2*, 131–137. [[CrossRef](#)]
24. Takashima, T.; Yokoyama, C.; Mizuma, H.; Yamanaka, H.; Wada, Y.; Onoe, K.; Nagata, H.; Tazawa, S.; Doi, H.; Takahashi, K.; et al. Developmental changes in P-glycoprotein function in the blood-brain barrier of nonhuman primates: PET study with R-¹¹C-verapamil and ¹¹C-oseltamivir. *J. Nucl. Med.* **2011**, *52*, 950–957. [[CrossRef](#)] [[PubMed](#)]

25. Kushihara, H.; Suzuki, H.; Terasaki, T.; Kakee, A.; Lemaire, M.; Sugiyama, Y. P-glycoprotein mediates the efflux of quinidine across the blood-brain barrier. *J. Pharmacol. Exp. Ther.* **1997**, *283*, 574–580.
26. Logan, J.; Fowler, J.S.; Volkow, N.D.; Wolf, A.P.; Dewey, S.L.; Schlyer, D.J.; MacGregor, R.R.; Hitzemann, R.; Bendriem, B.; Gatley, S.J.; et al. Graphical analysis of reversible radioligand binding from time-activity measurements applied to [N - ^{11}C -methyl]-(-)-cocaine PET studies in human subjects. *J. Cereb. Blood Flow Metab.* **1990**, *10*, 740–747. [[CrossRef](#)] [[PubMed](#)]
27. Hernández Lozano, I.; Bauer, M.; Wulkersdorfer, B.; Traxl, A.; Philippe, C.; Weber, M.; Häusler, S.; Stieger, B.; Jäger, W.; Mairinger, S.; et al. Measurement of hepatic ABCB1 and ABCG2 transport activity with [^{11}C]tariquidar and PET in humans and mice. *Mol. Pharm.* **2020**, *17*, 316–326. [[CrossRef](#)] [[PubMed](#)]
28. Hernández Lozano, I.; Karch, R.; Bauer, M.; Blaickner, M.; Matsuda, A.; Wulkersdorfer, B.; Hacker, M.; Zeitlinger, M.; Langer, O. Towards improved pharmacokinetic models for the analysis of transporter-mediated hepatic disposition of drug molecules with positron emission tomography. *AAPS. J.* **2019**, *21*, 61. [[CrossRef](#)] [[PubMed](#)]
29. Kamiie, J.; Ohtsuki, S.; Iwase, R.; Ohmine, K.; Katsukura, Y.; Yanai, K.; Sekine, Y.; Uchida, Y.; Ito, S.; Terasaki, T. Quantitative atlas of membrane transporter proteins: Development and application of a highly sensitive simultaneous LC/MS/MS method combined with novel in-silico peptide selection criteria. *Pharm. Res.* **2008**, *25*, 1469–1483. [[CrossRef](#)]
30. Zamek-Gliszczynski, M.J.; Kalvass, J.C.; Pollack, G.M.; Brouwer, K.L. Relationship between drug/metabolite exposure and impairment of excretory transport function. *Drug Metab. Dispos.* **2009**, *37*, 386–390. [[CrossRef](#)]
31. Munk, O.L.; Keiding, S.; Bass, L. Impulse-response function of splanchnic circulation with model-independent constraints: Theory and experimental validation. *Am. J. Physiol. Gastrointest. Liver Physiol.* **2003**, *285*, 671–680. [[CrossRef](#)]
32. Kawamura, K.; Yamasaki, T.; Konno, F.; Yui, J.; Hatori, A.; Yanamoto, K.; Wakizaka, H.; Takei, M.; Kimura, Y.; Fukumura, T.; et al. Evaluation of limiting brain penetration related to P-glycoprotein and breast cancer resistance protein using [^{11}C]GF120918 by PET in mice. *Mol. Imaging Biol.* **2011**, *13*, 152–160. [[CrossRef](#)] [[PubMed](#)]
33. Agarwal, S.; Uchida, Y.; Mittapalli, R.K.; Sane, R.; Terasaki, T.; Elmquist, W.F. Quantitative proteomics of transporter expression in brain capillary endothelial cells isolated from P-glycoprotein (P-gp), breast cancer resistance protein (Bcrp), and P-gp/Bcrp knockout mice. *Drug Metab. Dispos.* **2012**, *40*, 1164–1169. [[CrossRef](#)] [[PubMed](#)]
34. Wang, R.; Chen, H.L.; Liu, L.; Sheps, J.A.; Phillips, M.J.; Ling, V. Compensatory role of P-glycoproteins in knockout mice lacking the bile salt export pump. *Hepatology* **2009**, *50*, 948–956. [[CrossRef](#)]
35. Mennone, A.; Soroka, C.J.; Harry, K.M.; Boyer, J.L. Role of breast cancer resistance protein in the adaptive response to cholestasis. *Drug Metab. Dispos.* **2010**, *38*, 1673–1678. [[CrossRef](#)]
36. Fallon, J.K.; Smith, P.C.; Xia, C.Q.; Kim, M.S. Quantification of four efflux drug transporters in liver and kidney across species using targeted quantitative proteomics by isotope dilution nanoLC-MS/MS. *Pharm. Res.* **2016**, *33*, 2280–2288. [[CrossRef](#)] [[PubMed](#)]
37. Badawi, R.D.; Shi, H.; Hu, P.; Chen, S.; Xu, T.; Price, P.M.; Ding, Y.; Spencer, B.A.; Nardo, L.; Liu, W.; et al. First human imaging studies with the EXPLORER total-body PET scanner. *J. Nucl. Med.* **2019**, *60*, 299–303. [[CrossRef](#)]